This paper describes objective technical results and analysis. Any subjective views or opinions that might be expressed in the paper do not necessarily represent the views of the U.S. Department of Energy or the United States Government.

SAND2022-0060C

Model Validation of Falling Particle Receivers with On-sun Experiments

Brantley Mills[a,1)], Kevin Albrecht[a)], Luis F. González-Portillo[b)], and Clifford K. Ho[a)]

[a)]*Sandia National Laboratories, P.O. Box 5800, MS-0836, Albuquerque, NM 87185-0836, USA*
[b)]*Universidad Politécnica de Madrid, Madrid, Spain*

[1)]Corresponding author: bramill@sandia.gov

Abstract. Falling particle receivers are a promising receiver design to couple with particle-based concentrating solar power to help meet future levelized cost of electricity targets in next generation systems. The thermal performance of receivers is critical to the economics of the overall system, and accurate models of particle receivers are necessary to predict the performance in all conditions. A model validation study was performed using falling particle receiver data recently collected at the National Solar Thermal Test Facility at Sandia National Laboratories. The particle outlet temperature, the thermal efficiency of the receiver, and the wind speed and direction around the receiver were measured in 26 steady-state experiments and compared to a corresponding receiver model. The results of this study showed improved agreement with the experimental data over past validation efforts but did not fully meet all predefined validation metrics. Future model improvements were identified to continue to strengthen the modeling capabilities.

INTRODUCTION

The particle pathway is a leading technology for next-generation concentrating solar power (CSP) energy generation targeting a levelized cost of electricity (LCOE) of $0.05/kWh [1]. Particles offer a number of advantages over alternative technologies including: low parasitics, the ability to eliminate flux limitations on receiver tubing in fluid systems, the ability to directly store energy as sensible energy, and the absence of trace heating. Research is ongoing for various particle-based components including particle storage and particle heat exchangers to facilitate inexpensive electricity generation for a future CSP plant, but the focus of this paper is on the particle receiver. Different particle receiver designs have been proposed and tested including: the falling particle receiver (FPR) and its derivatives [2-4], the centrifugal CentRec® particle receiver [5], and the fluidized bed particle receiver [6]. This paper will specifically focus on the FPR concept designed and tested at the National Solar Thermal Test Facility (NSTTF) at Sandia National Laboratories.

A FPR is a cavity-type receiver in which a curtain of particles is released and falls via gravity past the beam of concentrated sunlight. In addition to being conceptually simple, FPRs have several advantages. First, a FPR enables direct irradiation of the falling particles eliminating the flux limitations of tubular systems. Second, existing north-facing FPR prototypes have been experimentally demonstrated to achieve average particle outlet temperatures exceeding 700°C [7]. Third, FPRs typically only require a slide gate to control the flow of particles falling through the receiver cavity (which could be PID controlled to maintain particle outlet temperatures in response to transients [8]). Finally, FPRs may also feature various obstructions in the particle curtain flow path that can increase particle volume fractions, curtain opacity, and residence time within the beam [4, 9, 10].

FPRs have some disadvantages when an open aperture is used in the design. First, an open aperture enables advective heat exchange between the hot air inside the cavity and the significantly cooler (and denser) ambient air. This can have an outsized impact on the thermal performance of a design as heated air escapes the cavity and is often the primary heat loss mechanism [11]. Furthermore, an open aperture also enables wind to increase the advective losses under specific conditions. Some of these effects can be mitigated through integrated design features [3]. Quartz

Sandia National Laboratories is a multimission laboratory managed and operated by National Technology & Engineering Solutions of Sandia, LLC, a wholly owned subsidiary of Honeywell International Inc., for the U.S. Department of Energy's National Nuclear Security Administration under contract DE-NA0003525.

aperture covers have also been explored to fully or partially cover the aperture though uncertainty in the scalability of this concept to commercial sized FPRs is an open question [12].

These disadvantages necessitate accurate FPR models to characterize the performance of a receiver. In addition, models provide a means of quickly interrogating the effect of different environmental conditions and changes to the design. Furthermore, validated models are critical to accurately assess the scalability of FPR technology and the receiver efficiency has been shown to be an important parameter in the LCOE from technoeconomic models [13]. This paper presents the results of a model validation study for a FPR modeling strategy using data collected from a recent experimental test campaign at the NSTTF at Sandia National Laboratories in 2020 and 2021.

Although there were several objectives in the 2020/21 NSTTF FPR test campaign, one critical objective of the testing was to collect quality model validation data for FPR models with and without various integrated design features aimed at improving the thermal performance. This experimental effort builds upon a previous test campaign in 2018 aimed at evaluating the thermal performance of the NSTTF receiver at that time. However, one key conclusion from the previous testing included the need to measure the speed and direction of wind more accurately during testing at the receiver for model validation efforts. Validating models of the FPR with the 2018 data was difficult since the receiver thermal efficiency was found to highly correlate with the wind conditions during a steady-state test which was not rigorously measured [11]. Therefore, additional wind instrumentation was implemented in the 2020/21 test campaign that serves to better characterize the free stream wind conditions and as validation metrics.

The remainder of this paper is summarized as follows. First, a description of the FPR experimental campaign is provided including the different receiver variations that were studied. Then, the computational model used to predict the thermal performance of the FPR used in the experiments is described. Next, comparisons between the experiments and the simulations are provided to build confidence in the modeling capability. Finally, the results and conclusions of this study are summarized.

RECEIVER TEST CAMPAIGN

The existing FPR system is located on the top of the 61 m solar tower at the NSTTF depicted in Fig. 1. In the tests, particles fall in a curtain through the north-facing receiver cavity and are returned to a feed hopper above the cavity via an Olds elevator behind the receiver. The structure housing the receiver and supporting elements is referred to here as the receiver module. A linearly actuated slide gate regulated the particle flow from the feed hopper into the cavity. The NSTTF heliostat field is used to irradiate the particles as they fall through the receiver. Heat rejection from the particles is not available in this flow loop. As a result, true steady-state experiments are not achievable as the particle inlet temperature will continue to rise as the experiment progresses. Instead, pseudo steady-state experiments are performed in which a brief time interval during operation is selected to represent steady-state conditions. However, this does introduce error into the validation process which uses steady-state simulations to compare with experimental data.

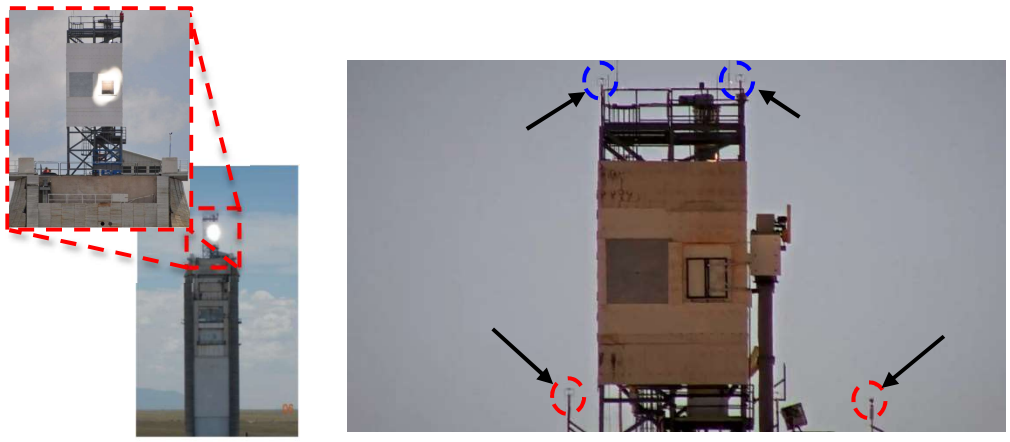

FIGURE 1. Receiver module atop the 61 m solar tower during an experiment (left) with 3D anemometers placed around the receiver module (right). Anemometers at the top of the receiver module (blue) measured free-stream velocity, and anemometers below the module (red) were used for validation.

The average particle temperature is measured at the inlet and outlet of the receiver cavity. Five immersed

thermocouples in the feed hopper along the width of the curtain inlet measure the inlet particle temperature before particles enter the cavity. Particle collection troughs containing thermocouples measure the particle temperature after passing through the beam at five points along the curtain width. The troughs are designed to ensure the thermocouples remain immersed in particles but do not accumulate and cause a lag in the particle temperature measurement. A water/glycol cooled panel adjacent to the FPR featuring a Lambertian surface is used to measure the power supplied to the receiver from the heliostat field. A Kendall radiometer is used to measure the peak flux and calibrate the spatial intensity of the beam. More details about this process are found in [7]. The particle mass flow rate is measured using load cells on the feed hopper to calculate the change in mass over time.

The experimental thermal efficiency of the FPR during pseudo steady-state conditions is then computed as follows:

$$\eta_{th} = \frac{Q_{abs}}{Q_{in}} = \frac{\dot{m}\left(h_{out} - h_{in}\right)}{Q_{in}} = \frac{\dot{m}\int_{T_{in}}^{T_{out}} c_P\left(T\right)dT}{Q_{in}} \tag{1}$$

where Q_{abs} is the absorbed thermal power in the particles, Q_{in} is the incident radiative power entering the cavity, $\dot{m}$ is the particle mass flow rate, h is the particle enthalpy, and $c_P\left(T\right)$ is the particle specific heat as a function of the average particle temperature, T which is defined as:

$$c_P\left(T\right) = 388.4 \cdot T^{0.1523} \tag{2}$$

where the fit for the specific heat is derived from Georgia Tech's Thermophysical Properties Database [14].

As discussed above, five 3D anemometers were placed around the receiver module to measure the wind speed and direction. Two anemometers were placed at the top of the receiver module (c.f. Fig. 1) to be more representative of the free-stream wind conditions. Three anemometers were placed to the east, west, and south of the receiver module to use as validation metrics for the wind conditions created by the presence of the module itself. The location of these anemometers was selected based on the proximity to the receiver cavity while avoiding spillage from the beam that would damage the instrumentation.

In addition to anemometers, this test campaign featured a truncated receiver cavity geometry and the addition of a "catch and release" trough in the particle curtain flow (i.e. a multistage receiver [3]). Both features were intended to increase the thermal performance of the receiver compared to the original 2018 geometry. From the experimental dataset, 26 pseudo steady-state cases were selected for the validation study: 10 cases of the receiver featuring a free-falling curtain with truncation only and 16 cases with a single trough in the flow path. Although additional cases were available, several cases were excluded due to incomplete data, lower incident radiative powers where the experimental uncertainty was higher (<350 kW), and uncertainty in the accuracy of some critical measurements.

COMPUTATIONAL MODEL

The modeling strategy applied in this validation study uses a Lagrangian–Eulerian framework within the ANSYS Fluent® simulation code. A simplified geometric representation of the receiver module atop the tower is used in the computational model as depicted in Fig. 2a. To minimize the number of elements required in the domain, only the profile of module is included at the expense of increased accuracy of the velocity field around the module particularly in the wake. The NSTTF tower is also excluded from the domain assuming minimal effects with the receiver cavity. The receiver cavity with a freefall configuration and a single trough configuration are depicted in Fig. 2b and Fig. 2c, respectively. A tetrahedral mesh of with ~2.5 million elements is used for the simulations with variable mesh sizing following similarly sized FPR models [11, 15]. In addition to improved measurements of the wind speed and direction in the experiments, key differences in the models over those used in previous validation studies [11] include a larger computational domain and the inclusion of the simplified receiver module. Furthermore, a more accurate representation of the cavity and particles bouncing within the bottom hopper are also included in this latest version of the model to more accurately capture the velocity field inside the cavity.

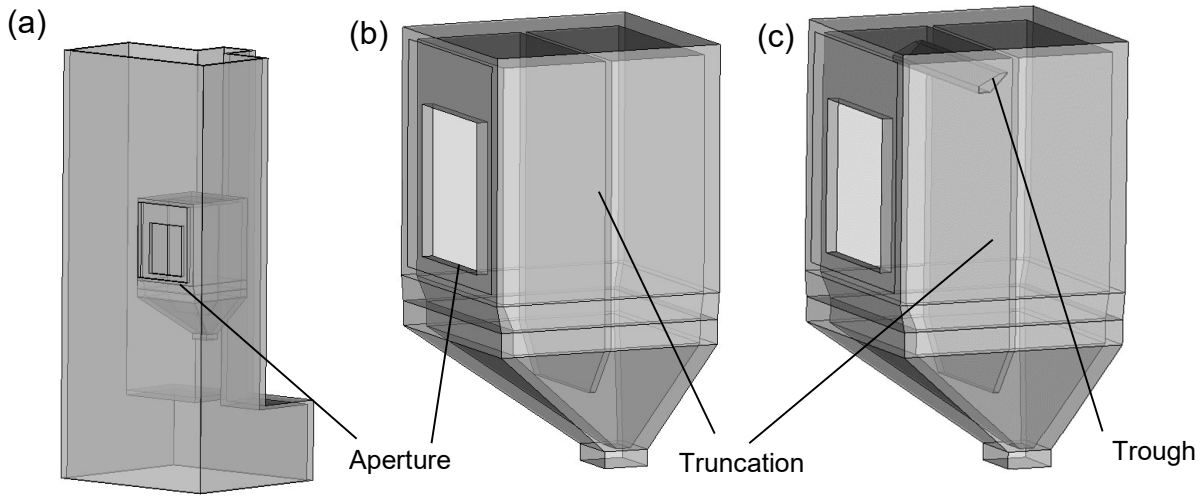

FIGURE 2. Solid model depiction of the receiver and module atop the tower (a), the receiver cavity with the cavity truncation (b) and the receiver cavity with the cavity truncation and a single catch and release trough (c).

In the Lagrangian-Eulerian framework, discrete particle parcels are injected into the domain at the top of the receiver and fall via gravity through the air continuum. The air is modeled inside and outside of the receiver cavity and coupled with the particles through drag forces, heat transfer, and turbulent interactions using constitutive relationships within Fluent. Particles are modeled as spherical CARBO-HSP 40/70 with a nominal diameter of 350 μm using thermal properties from [14, 16]. A realizable k-ε turbulence model [17] is implemented in the air continuum using Fluent's scalable wall functions [18] to provide a degree of mesh insensitivity for the turbulent wall interactions.

A non-grey, discrete ordinates (DO) radiation model is coupled with the computational fluid dynamics model to include radiative transport into the receiver from the heliostat field. The non-grey model is divided into three bands: 0.1–2.5 μm, 2.5–4.5 μm, and 4.5–100 μm. All incident solar irradiance enters the domain in the smallest wavelength band. The two longer wavelength bands correspond to the thermal wavelengths with a demarcation between them defined by different emissivities in the alumina silica fiberboard walls inside the receiver.

Ray-tracing simulations using NREL's SolTrace v3.1 package are leveraged to simulate the direction and intensity of the radiation from the NSTTF heliostat field during testing. A model of the solar radiation passing through the north face of the computational domain from a subset of the NSTTF heliostats is created. The ray tracing model is based upon previously used models of the NSTTF field [19], and each of the heliostats is modeled with a reflectivity, slope error, and specularity error of 0.885, 1.2 mrad, and 0.05 mrad, respectively. A total of 1×10^7 ray intersections are generated and a DNI of 1000 W/m^2 is assumed. From the radiation vectors passing through the north surface, analytical expressions are fit to spatially describe the directionality and intensity of the beam. The expressions are simply a product of trigonometric and exponential functions that best captures the spatial variation in the field from visualization of the results. The fitted expressions are implemented in the model as user defined functions and the intensity is scaled proportionally to match flux values measured in each experiment.

Particle-to-particle collisions are ignored in the falling curtain under the assumption that the particle volume fraction in the curtain is small [16]. However, reduced order models are used to simplify the particle interaction physics with the stagnant particles in the trough under steady-state conditions. The modeling approach is described in detail in [9]. In short, this model treats the bed of particles in a trough as a solid with an angle of repose matching the physical properties of the particles (30°). Particles that collide with the bed rebound with a fixed velocity that is calibrated to match experimental results observed in a cold flow test rig [20]. Some effects are not captured in this model including the lateral curtain spread from particles leaving the trough, which may affect how the average particle outlet temperature is computed for each experiment

The FPR thermal efficiency is computed in the simulations by averaging the particle temperatures at the elevation of the particle collection troughs and using Eq. (1). Free-stream wind speed and direction during an experiment are input as velocity boundary conditions on the appropriate exterior domain surfaces as measured by an average of the top two anemometers in the experiment. Other boundaries within the domain are assigned as pressure boundaries. The wind speed and direction from the other three anemometer locations are extracted for comparison with the

experimental data. The anemometer locations within the computational domain are depicted in Fig. 3. A single steady-state simulation of an experiment using approximately 96 CPU cores takes approximately 24 hours to converge.

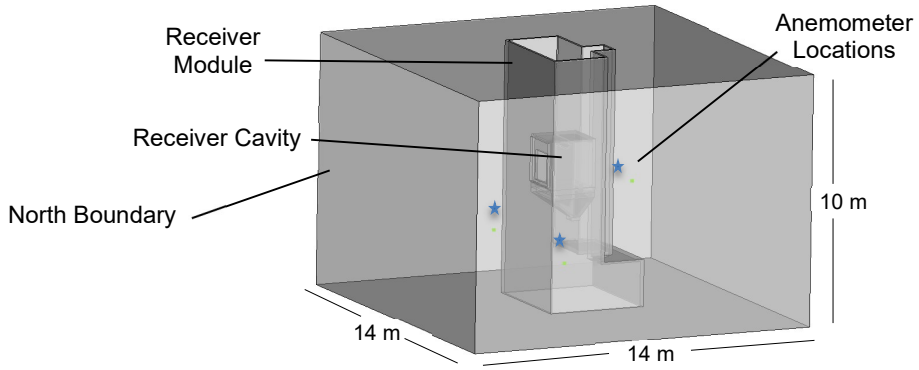

FIGURE 3. A dimensioned solid model of the computational domain. Stars indicate the location of the anemometer instrumentation.

MODEL VALIDATION STUDY

For each of the 26 validation cases, the measured incident radiative power, particle mass flow rate, particle inlet temperature, free-stream wind speed and direction are simulated. The particle outlet temperature, thermal efficiency, wind speed and direction at the lower three anemometer locations are calculated by the model to compare with the experiments for a total of 8 validation metrics. Parity plots between the experimentally measured values and the simulations results are created. If the simulation and the experiments agree perfectly in a parity plot, all the data follows the line y = x.

Linear fits of the data in each parity plot are created to objectively evaluate how well the simulations predict the experimental results. The slope and the coefficient of determination, R^2, of the fit are used as metrics to evaluate the models. For this study, a slope between 0.75 and 1.25 with an $R^2 > 0.75$ is targeted for a successful validation based on estimates of sufficient accuracy for the FPR response from expert judgement and historical precedent. Parity plots of the particle outlet temperature and thermal efficiency for the multistage configuration and freefall configuration are provided in Fig. 4 and Fig. 5, respectively. A slope of 0.48 with an R^2 of 0.66 is observed for the multistage cases, and a slope of 0.51 with an R^2 of 0.65 is observed for the freefall cases. Although there is still significant scatter in the plots as seen by R^2, compared to a previous validation effort (slope of 0.11 with an R^2 of 0.08 [11]), this represents a considerable improvement and builds confidence that these models can predict the thermal performance of FPRs. Models of multistage cases shown in Fig. 4 show a consistent underprediction in the particle outlet temperature and thermal efficiency compared with the experimental data (hence the decision to separate the receiver configurations into separate parity plots). Presently, this is explained by the simplified physics applied in the models for the complex particle behavior created by the multistage features. For example, any lateral spread in the curtain (i.e. east/west) would not be captured in the models but may be reflected in the particle temperature measurements. In that scenario, hotter particles in the center of the curtain would be more likely to be measured in the fixed particle outlet troughs compared to a free-falling curtain. Improved models for the multistage physics may show better predictions and will be explored in the future. Additional disagreement between the experiments and the simulations may also be explained by the pseudo steady-state nature of the experiments where inconsistent heating and cooling of the refractory walls prior to measurements may not be captured by the steady-state models. The magnitude of this effect is an active area of study and will be mitigated by future systems that enable full steady-state experiments.

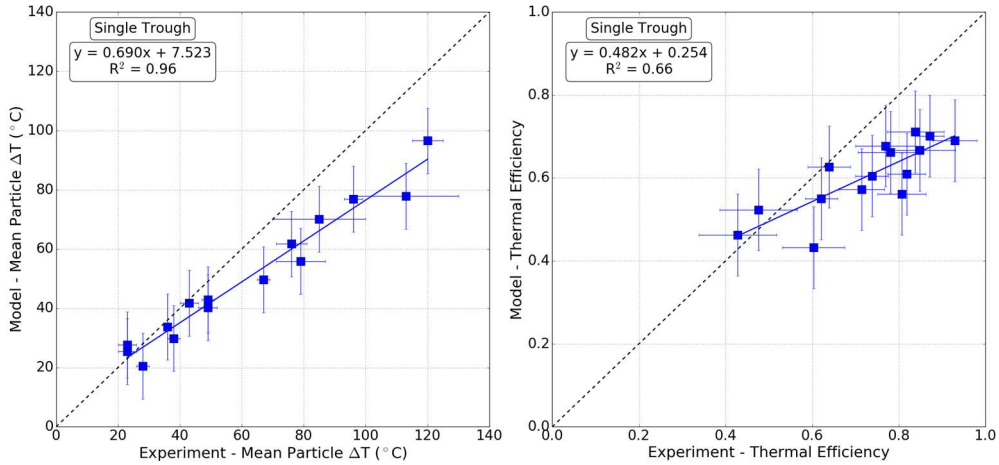

FIGURE 4. Parity plot of the particle outlet temperature and the receiver efficiency with multistage features

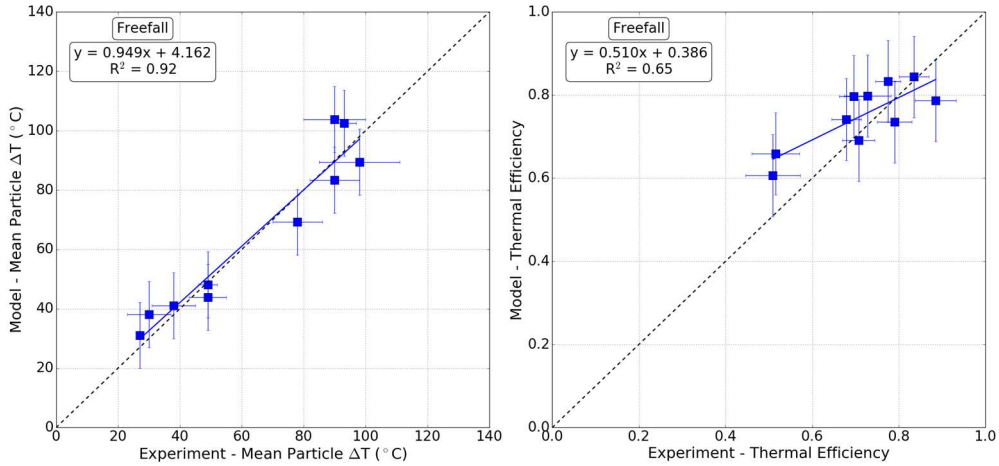

FIGURE 5. Parity plot of the particle outlet temperature and the receiver efficiency without multistage features.

The parity plots for the wind speed and direction for the west, east, and south anemometer locations are shown in Fig. 6, Fig. 7, and Fig. 8, respectively. Note that the different receiver configurations are not separated into individual plots as the effect on the wind around the receiver module from differences in the geometry are likely negligible. Considerable scatter is observed in the plots for wind (possibly from using point measurements for wind in these locations), with the best overall agreement observed in the west anemometer location. As the NSTTF winds tend to originate from the west, this location is the least sensitive to the wake created by the receiver module and comparisons at this location experience less variability. More scatter is observed in the wind direction at the east and south locations likely exaggerated by simplifications made to the geometry of the receiver module as shown in Fig. 2a. Improved geometric fidelity is recommended to improve models of wind conditions around the receiver at the expense of higher computational cost.

In summary, of the 10 parity plots shown in Fig. 4 through Fig. 8, 30% of the metrics met the validation criteria for the slope and R^2 in the linear fits. Alternatively, 90% of the metrics are within 0.25 of the validation metrics for the slope and R^2 suggesting that there is room for improvement. Improved physical models for the multistage configurations, additional geometric fidelity in the receiver module, and full steady-state experiments offer some areas where the validation can be improved.

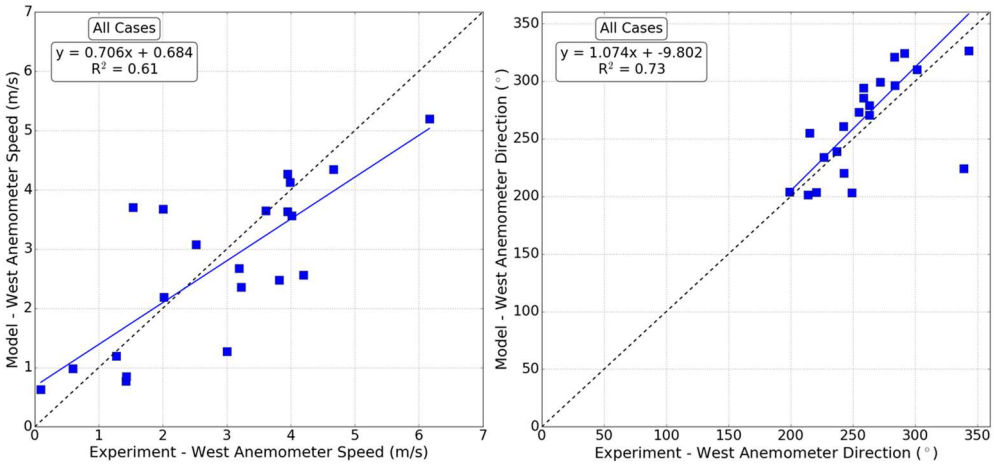

FIGURE 6. Parity plot of the wind speed and direction at the west anemometer location.

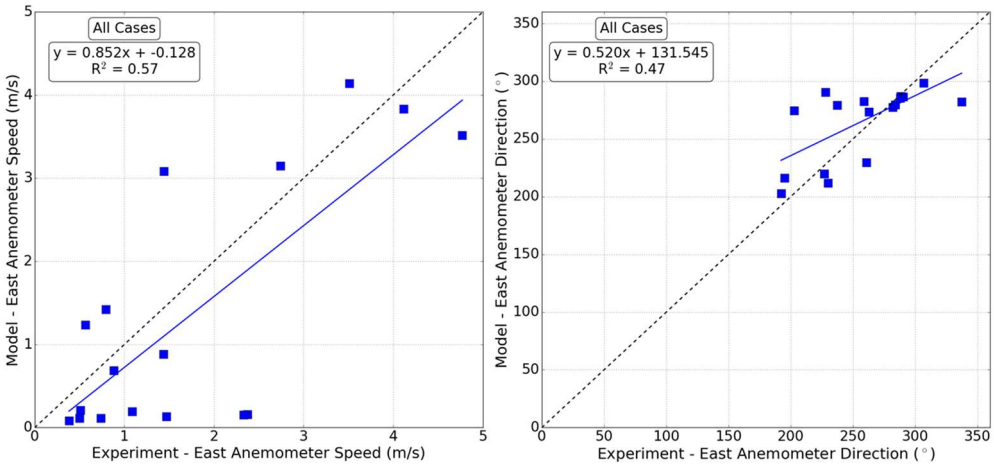

FIGURE 7. Parity plot of the wind speed and direction at the east anemometer location.

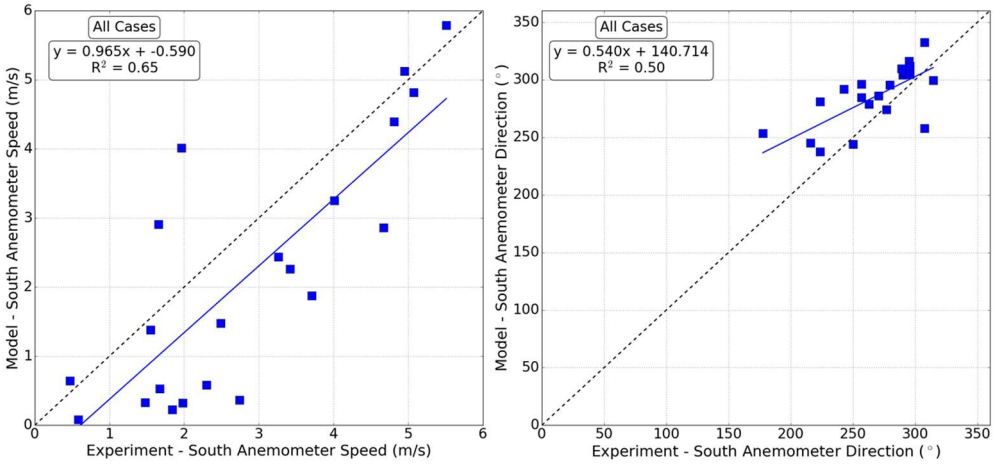

FIGURE 8. Parity plot of the wind speed and direction at the south anemometer location.

CONCLUSIONS

A model validation study was performed on a falling particle receiver model utilizing recently collected data for the existing receiver system at the National Solar Thermal Test Facility at Sandia National Laboratories. The average particle outlet temperature and the thermal efficiency for two receiver configurations were experimentally measured and used as validation metrics. In addition, local anemometer measurements for wind speed and direction around the receiver system were also measured for validation. Models of the receiver configurations were created and the experimentally measured conditions for 26 steady-state experiments were simulated. Parity plots between the experimental data and the simulated results were created. Linear fits of the data in these plots were generated to evaluate the models based on the slope and R^2 of those fits. Improved measurements of the wind during experiments and other model enhancements provided significantly better agreement between models and experiments than in previous validation studies. However , only 30% of the validation metrics fully meet the criteria set forth at the onset of the study. Areas of improvement included models used to simulate the particle dynamics of multistage receiver designs, increased geometrical fidelity in the module supporting the falling particle receiver system, and full steady-state experiments.

ACKNOWLEDGMENTS

This work was funded in part or whole by the U.S. Department of Energy Solar Energy Technologies Office under Award Number 37372. This report was prepared as an account of work sponsored by an agency of the United States Government. Neither the United States Government nor any agency thereof, nor any of their employees, makes any warranty, express or implied, or assumes any legal liability or responsibility for the accuracy, completeness, or usefulness of any information, apparatus, product, or process disclosed, or represents that its use would not infringe privately owned rights. References herein to any specific commercial product, process, or service by trade name, trademark, manufacturer, or otherwise does not necessarily constitute or imply its endorsement, recommendation, or favoring by the United States Government or any agency thereof. The views and opinions of authors expressed herein do not necessarily state or reflect those of the United States Government or any agency thereof.

Sandia National Laboratories is a multi-mission laboratory managed and operated by National Technology and Engineering Solutions of Sandia, LLC., a wholly owned subsidiary of Honeywell International, Inc., for the U.S. Department of Energy's National Nuclear Security Administration under contract DE-NA0003525.

REFERENCES

1. Generation 3 Concentrating Solar Power Systems (Gen3 CSP) Phase 3 Project Selection, 2021. https://www.energy.gov/eere/solar/generation-3-concentrating-solar-power-systems-gen3-csp-phase-3-project-selection. (Accessed December 13, 2021).
2. Ho, C.K., Christian, J.M., Yellowhair, J.E., Armijo, K., Kolb, W.J., Jeter, S., Golob, M., Nguyen, C., 2019, "On-Sun Performance Evaluation of Alternative High-Temperature Falling Particle Receiver Designs", Journal of Solar Energy Engineering, 141(1), p. 011009 (7 pages). DOI: 10.1115/1.4041100
3. Mills, B., Shaeffer, R., Yue, L., Ho, C.K., 2020, "Improving Next-Generation Falling Particle Receiver Designs Subject to Anticipated Operating Conditions", ASME 2020 14th International Conference on Energy Sustainability, ES2020-1667, Virtual Online Conference, June 17 - 18, 2020.
4. Al-Ansary, H., El-Leathy, A., Jeter, S., Djajadiwinata, E., Alaqel, S., Golob, M., Nguyen, C., Saad, R., Shafiq, T., Danish, S., Abdel-Khalik, S., Al-Suhaibani, Z., Abu-Shikhah, N., Haq, M.I., Al-Balawi, A., Al-Harthi, F., 2018, "On-Sun Experiments on a Particle Heating Receiver with Red Sand as the Working Medium", AIP Conference Proceedings, 2033, p. 040002 (8 pages). DOI: 10.1063/1.5067038
5. Ebert, M., Amsbeck, L., Rheinländer, J., Schlögl-Knothe, B., Schmitz, S., Sibum, M., Uhlig, R., Buck, R., 2019, "Operational Experience of a Centrifugal Particle Receiver Prototype", AIP Conference Proceedings, 2126, p. 030018 (8 pages). DOI: 10.1063/1.5117530
6. Deng, Y., Sabatier, F., Dewil, R., Flamant, G., Gal, A.L., Gueguen, R., Baeyens, J., Li, S., Ansart, R., 2021, "Dense upflow fluidized bed (DUFB) solar receivers of high aspect ratio: Different fluidization modes through inserting bubble rupture promoters", Chemical Engineering Journal, 418, 129376. DOI: 10.1016/j.cej.2021.129376

7. Ho, C.K., Schroeder, N.R., Labuscher, H.L., Yue, L., Mills, B., Shaeffer, R., Christian, J.M., Albrecht, K.J., 2020,"Receiver Design and On-Sun Testing for G3P3-USA", SolarPACES 2020, Virtual Online Conference.
8. Ho, C.K., Peacock, G., Christian, J.M., Albrecht, K.J., Yellowhair, J.E., Ray, D., 2019, "On-Sun Testing of a 1 MW_t Particle Receiver with Automated Particle Mass-Flow and Temperature Control", AIP Conference Proceedings, 2126, p. 030027 (9 pages). DOI: 10.1063/1.5117539
9. Shaeffer, R., Mills, B., Yue, L., Ho, C.K., 2020, "Evaluation of Performance Factors for a Multistage Falling Particle Receiver", ASME 2020 14th International Conference on Energy Sustainability, ES2020-9783, Virtual Online Conference, June 17 - 18, 2020. DOI: 10.1115/ES2020-1692
10. Kim, J.-S., Kumar, A., Gardner, W., Lipiński, W., 2019, "Numerical and Experimental Investigation of a Novel Multi-Stage Falling Particle Receiver", AIP Conference Proceedings, 2126, p. 030030 (8 pages). DOI: 10.1063/1.5117542
11. Mills, B., Ho, C.K., 2019, "Simulation and performance evaluation of on-sun particle receiver tests", AIP Conference Proceedings, 2126, p. 030036 (8 pages). DOI: 10.1063/1.5117548
12. Yue, L., Mills, B., Ho, C.K., 2019, "Effect of Quartz Aperture Covers on the Fluid Dynamics and Thermal Efficiency of Falling Particle Receivers", ASME 2019 13th International Conference on Energy Sustainability, ES2019-3910, Bellevue, Washington, USA, July 14–17, 2019. DOI: 10.1115/ES2019-3910
13. González-Portillo, L.F., Albrecht, K.J., Ho, C.K., 2021, "Techno-economic optimization of CSP plants with free-falling particle receivers", Entropy, 23(1), p. 76. DOI: 10.3390/e23010076
14. Thermophysical Properties Database of Gen3 CSP Materials, 2021. http://gen3csp.gatech.edu/.
15. Mills, B., Schroeder, B., Yue, L., Shaeffer, R., Ho, C.K., 2019, "Optimizing a Falling Particle Receiver Geometry Using CFD Simulations to Maximize the Thermal Efficiency", AIP Conference Proceedings, 2303, p. 030027 (11 pages). DOI: 10.1063/5.0029331
16. Siegel, N.P., Ho, C.K., Khalsa, S.S., Kolb, G.J., 2010, "Development and evaluation of a prototype solid particle receiver: On-sun testing and model validation", Journal of Solar Energy Engineering, 132(2), p. 021008 (8 pages). DOI: 10.1115/1.4001146
17. Shih, T.-H., Liou, W.W., Shabbir, A., Yang, Z., Zhu, J., 1995, "A New k-ϵ Eddy Viscosity Model for High Reynolds Number Turbulent Flows", Computers & Fluids, 24(3), pp. 227-238. DOI: 10.1016/0045-7930(94)00032-T
18. ANSYS® Fluent® Theory Guide", Help System, ANSYS, Inc.
19. Yellowhair, J., Ho, C.K., 2019, "Optical ray-tracing performance modeling of quartz half-shell tubes aperture cover for falling particle receiver", ASME 2019 13th International Conference on Energy Sustainability, ES2019-3927, Bellevue, WA, USA. DOI: 10.1115/ES2019-3927
20. Yue, L., Schroeder, N., Ho, C.K., 2020, "Particle Flow Testing of a Multistage Falling Particle Receiver Concept: Staggered Angle Iron Receiver (StAIR)", ASME 2020 14th International Conference on Energy Sustainability, ES2020-1666, Virtual Online Conference, June 17 - 18, 2020. DOI: 10.1115/ES2020-1666